**Geomechanics and Engineering**, *Vol. 27, No. 3 (2021) 263-271*
https://doi.org/10.12989/gae.2021.27.3.263


# Numerical research on two-dimensional bridge formation at the cohesionless sand-geotextile interface with the DEM method

Sheng Liu[1a], Yuan Wang[1b] and Di Feng*[2]

[1]*College of Water Conservancy and Hydropower Engineering, Hohai University, Nanjing 210098, China*
[2]*College of Civil and Transportation Engineering, Hohai University, Nanjing 210098, China*

*(Received July 31, 2020, Revised October 9, 2021, Accepted October 13, 2021)*

**Abstract.** Soil particles may be blocked at the pores of geotextiles even if the diameter of the soil particle is smaller than the size of the pores, and then a soil bridge is formed. To design a reasonable filter, it is vital to understand the formation of bridges at the soil-geotextile interface. The two-dimensional Distinct-Element Method was used to explore bridge formation at the cohesionless sand-geotextile interface. To realistically reflect the geological environment of cohesionless sand, the hydraulic gradient, confining pressure, multiple openings and inherent characteristics of cohesionless sand were covered in the simulations. It is found that both the number of openings of the filter and the uniformity coefficient of cohesionless sand had a substantial influence on the formation of a soil bridge. The bridge coefficient substantially decreased when there was more than one opening, because the narrower walls decreased the support of the bridge foot. When the confining pressure was greater than zero, the bridge coefficient was larger than that when there was no confining pressure. With the continual increase in the confining pressure, the confining pressure began to have an unfavourable effect on the formation of a soil bridge. The hydraulic gradient slightly decreased the bridge coefficient when the uniformity coefficient was 1.

**Keywords:** bridge formation; cohesionless sand; DEM method; geotextile; two-dimensional

## 1. Introduction

Geosynthetics have been widely used in engineering for filtration, separation, reinforcement, etc. (Liu *et al*. 2021, Raja and Shukla 2020, Raja and Shukla 2021a, Raja and Shukla 2021b) due to the advantages of convenience of use and installation, low environmental impact, and low cost. The aim of a geotextile filter is to permit the free flow of water from in situ soil to a drain without allowing substantial long-term loss of the soil particles. The pore size of the geotextile filter is the key parameter during the design of filter. The pore size of the geotextile filter must meet retention criterion, and the basic mechanism of the retention criterion is given in Eq. (1) (Liu and Xie 2017). The core idea of the retention criterion of filter material is to retain the controlling diameter of the protected soil with the pore size of the filter. Meanwhile, the bridge formation of the protected soil at the soil-geotextile interface must be considered (Giroud 2010). The soil particles may be blocked at the pores of geotextiles even if the diameter of the soil particle is smaller than the size of the pore, and then a soil bridge is formed (Khan *et al*. 2018, Watson and John 1999). For simplification, the bridge coefficient in the design criteria of a filter is usually taken as 1-2 (Liu and Xie 2017). In reality, the bridge coefficient greatly varies on different occasions. To design a reasonable filter, it is vital to understand the formation of bridges at the soil-geotextile interface.

$$D_0 \le \alpha d_k \tag{1}$$

where $D_0$ is the average pore diameter of the filter material, $d_k$ is the controlling diameter of the protected soil, and $\alpha$ is the bridge coefficient.

An increasing number of scholars have begun to focus on the bridge formation of granular materials (Guerrero *et al*. 2019, Lozano *et al*. 2015, Parretta and Grillo 2019). However, only limited research has considered the influence of the confining pressure and multiple openings on bridge formation. A series of tests was devised by Watson and John (1999) to examine the formation of soil particle bridges on the surface of non-compressible woven and non-woven geotextiles, and the relationship between the uniformity coefficient, particle size and pore size was examined. Valdes and Santamarina (2008) investigated the pore-scale mechanisms involved in bridge formation and destabilization with an experimental method and focused on the influence of the particle shape on the maximum throat-to-particle size ratio. However, these studies did not cover the influence of the confining pressure and multiple openings on bridge formation. Concerning the bridge formation of grains, most previous experimental and simulation studies on the jamming of a silo have focused on a single outlet. However, Mondal and Sharma (2014) presented a simulation study on the formation of particle arches supported by flying buttresses through two adjacent

*Corresponding author, Associate professor
E-mail: fengdi@126.com
[a] Ph.D.
E-mail: liusheng3131@136.com
[b] Professor
E-mail: wangyuanhhu@163.com



ISSN: 2005-307X (Print), 2092-6219 (Online)

slots (rectangular outlets) and produced several new findings. A custom-made trapdoor test box was used to investigate the development of soil arching under localized surface static loading and cyclic loading (Xu *et al*. 2019b), but this research did not analyse the arch coefficient.

Fluids have an important influence on the bridge formation of soil particles (Liu *et al*. 2019, Valdes and Santamarina 2006). To study the influence of the seepage flow on soil arching, a series of two-dimensional trapdoor tests were carried out considering different fill heights and water level heights (Xu *et al*. 2019a), and it was found that seepage flow increased the displacement of the particles and the effective vertical stress acting at the top of the trapdoor. Jung *et al*. (2018) reported an approach using microfluidic pore models to study the migration of fine particles and the bridging/clogging behaviour in a structure mimicking porous media. The results from the microfluidic model showed that fine particles accumulated along the water and gas, and consequently, bridging and clogging occurred in the pore throat. However, little attention has been paid to the interaction between the arch coefficient and seepage flow. Li and Aubertin (Li and Aubertin 2009a, Li and Aubertin 2009b) conducted theoretical research on the soil arching effect in 3D backfilled openings under hydrostatic conditions, but the influence of seepage flow was not accounted for.

To better design a filter material that retains protected soil and drainage, it is vital to understand the formation of bridges at the soil-geotextile interface. According to the tests conducted by Watson and John (1999), the results of the bridge formation obtained from two-dimensional tests were equally valid for three-dimensional tests. Therefore, to promote high computational efficiency, the bridge formation of cohesionless sand was examined by the two-dimensional Distinct-Element Method (DEM) with an emphasis on the arch coefficient. The influence of the hydraulic gradient, confining pressure, multiple openings and inherent cohesionless characteristics (porosity, gradation and friction coefficient) on bridge formation was examined. The results from these simulations are relevant to filter clogging and unclogging, water and oil extraction, sand production in oil wells, and food grain, aggregate and powder handling operations.

## 2. Simulation method

### *2.1 Discrete element method*

The Distinct-Element Method (DEM) was introduced by Cundall (1971) for the analysis of rock mechanics problems and then applied to soils by Cundall and Strack (1979). A thorough description of this method is given in the two-part paper by Cundall (1988) and Hart *et al*. (1988). DEM simulations were carried out using PFC$^{2D}$ in this paper. The PFC programs provide a general purpose, distinct-element modelling framework that includes both a computational engine and a graphical user interface. The PFC model simulates the movement and interaction of many finite-sized particles. The particles are rigid bodies with finite mass that move independently of one another and can both translate and rotate. Particles interact at pairwise contacts by means of an internal force and moment. The contact mechanics are embodied in particle-interaction laws that update the internal forces and moments. The time evolution of this system is computed via the distinct-element method, which provides an explicit dynamic solution to Newton's laws of motion as follows:

$$\frac{\partial \vec{u}}{\partial t} = \frac{\vec{f}_{mech}}{m} + \vec{g} \tag{2}$$

$$\frac{\partial \vec{\omega}}{\partial t} = \frac{\vec{M}}{I} \tag{3}$$

where $\vec{u}$ is the particle velocity, $\vec{f}_{mech}$ is the sum of the additional forces (externally applied and contact forces) acting on the particle, m is the particle mass, $\vec{g}$ is the acceleration due to gravity, $\vec{\omega}$ is the particle angular velocity, $\vec{M}$ is the moment acting on the particle, and $I$ is the moment of inertia.

PFC provides a particle-flow model that contain the following assumptions: (1) The particles are treated as rigid bodies. (2) The fundamental particle shape is a disk with unit thickness in 2D and a sphere in 3D, denoted by a ball. (3) Particles interact at pairwise contacts by means of an internal force and moment. The contact mechanics are embodied in particle-interaction laws that update the internal forces and moments. (4) The behaviour at the physical contacts uses a soft-contact approach where the rigid particles are allowed to overlap one another at the contact points. The contacts occur over a vanishingly small area (i.e., at a point), and the magnitude of the overlap and/or the relative displacement at the contact point are related to the contact force via the force-displacement law.

In addition to balls, the PFC particle-flow model also includes walls. Walls allow one to apply velocity boundary conditions to assemblies of balls for purposes of compaction and confinement. The balls and walls interact with one another via the forces that arise at the contacts. The equations of motion are satisfied for each ball. However, the equations of motion are not satisfied for each wall. Instead, its motion is specified by the user and remains constant regardless of the contact forces acting on it. PFC has been successfully applied to a very broad range of numerical investigations.

### *2.2 Model formulation*

To obtain reasonable simulation results, it is first important to build a reasonable model. The specimens in a laboratory can be divided into two types: the specimen without a confining pressure and the specimen with a confining pressure, and they both have good homogeneity in general. To reproduce the specimen in the laboratory, this paper tries to build these two kinds of specimens. At present, the common way to construct a DEM model with a desired porosity is called the ball distribution method (BDM). In this method, a set of balls are created, and their positions and radii are drawn from uniform distributions throughout the model domain by default. This process

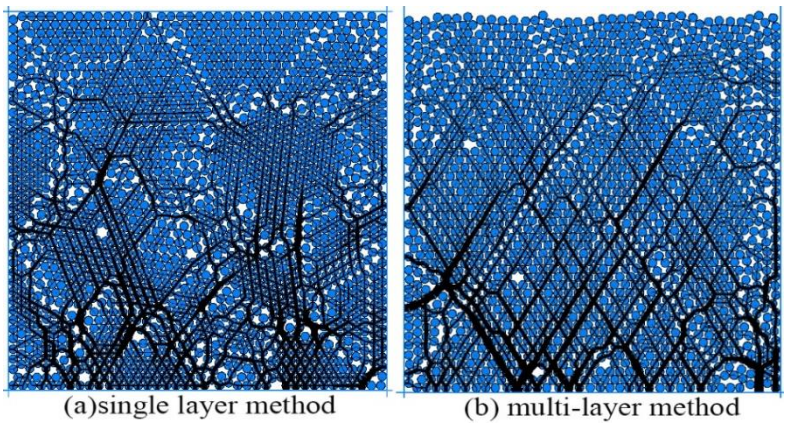


Fig. 1 Model obtained by different methods (length=4 mm, height=4 mm, and radius of the ball=0.05 mm)

ceases when a target porosity (not accounting for overlap) is achieved. The initial balls may overlap with other balls, and they bounce off each other due to their contact forces until a balanced state is achieved (the ratio of the average value of the unbalanced force over all the balls to the average value of the sum of the magnitudes of the contact forces, body forces and applied forces over all the balls is less than 1e-5). For the specimen without a confining pressure, the confining pressure is applied and maintained by the wall with servo control (Zhang *et al*. 2017). For the specimen without a confining pressure, the practical stress in the soil increases with increasing depth. To reproduce the gravity gradient field, the balls are calculated to a balanced state with gravity and a normal friction coefficient. The friction of the ball is set to zero to increase the homogeneity of the specimen during these processes.

After many attempts, it is found that the numerical model built by the BDM in a single layer (SL) shows local heterogeneity (the porosity in the local area is too large or small), and it is difficult to guarantee the homogeneity of the specimen. A model built with a SL (Fig. 1(a)) is given as an example to elaborate this phenomenon. Both the friction coefficients of the balls and wall are set to 0.5. Twelve measuring circles (radius=0.5 mm) are installed to measure the porosity of the specimen (Fig. 3). The average porosity of the measuring circles of each row or column are calculated as a representative value and is shown in Fig. 3. It is clear that the porosity of the SL specimen shows a large discreteness.

To obtain a more uniform numerical model whose stress is in accordance with the practical stress distribution law, a multi-layer method (ML) is proposed. The process of constructing the model is summarized as follows:

(1) First, a set of non-overlapping balls were randomly generated in a given area, and the top wall was then moved down under a fixed velocity to compress the balls to a target porosity. After that, the top wall was fixed, and the balls were calculated to a balanced state. The first layer of balls was generated. It should be noted that during these processes, the gravity and the friction coefficient of the balls were set to zero. In addition, the balls exceeding the given area were deleted.

(2) A new blank area over the first layer was generated, and the second layer of non-overlapping balls was randomly generated in this area. The top wall was then moved down to compress the balls to a target porosity. Last, the wall between these two layers of balls was deleted, and the balls were calculated to a balanced state. The second layer of balls was generated.

(3) Step (2) was repeated until the specimen reached the predetermined height. Six layers of balls were generated in this paper.

(4) Gravity was set to 9.8 m/s$^2$, and the friction coefficient of the balls was set to the design value. The specimen was calculated to a balanced state, and the first and last layers of balls were deleted to make the specimen more uniform. Last, the specimen was obtained by calculating to a balanced state again.

Because of the existence of compaction energy during the process of compaction, the porosity of the first layer of balls was slightly smaller than the average value, and the porosity of the last layer of balls was slightly larger. To enhance the homogeneity of the specimen, the first and last layers were deleted in the last step of the model formulation process. Therefore, two more layers of balls should be generated during the model formulation process.

To compare the homogeneity of the specimen generated by a SL and ML, two models (Fig. 1) were built with these two methods. Both the friction coefficients of the balls and wall were set to 0.5 in the two models. Twelve measuring circles (radius=0.5 mm) were installed to measure the porosity of the specimen. The average porosity of the measuring circles of each row or column was calculated as a representative value and is shown in Fig. 3. It is clear that the porosity of the ML specimen showed a better homogeneity than that of the SL specimen.

Cohesionless sand was modelled in this paper, and the parameters of the model are given in Table 1 based on the literature (Li *et al*. 2017).

### *2.3 Simulation process*

To study the formation of a soil bridge at the cohesionless sand-geotextile interface, one or multiple identical openings are made at the middle of the bottom wall (Fig. 4). Similarly, as a three-dimensional pore can be idealized as a circle or as a rectangle, in two dimensions, it can be represented by a straight-line opening. For the

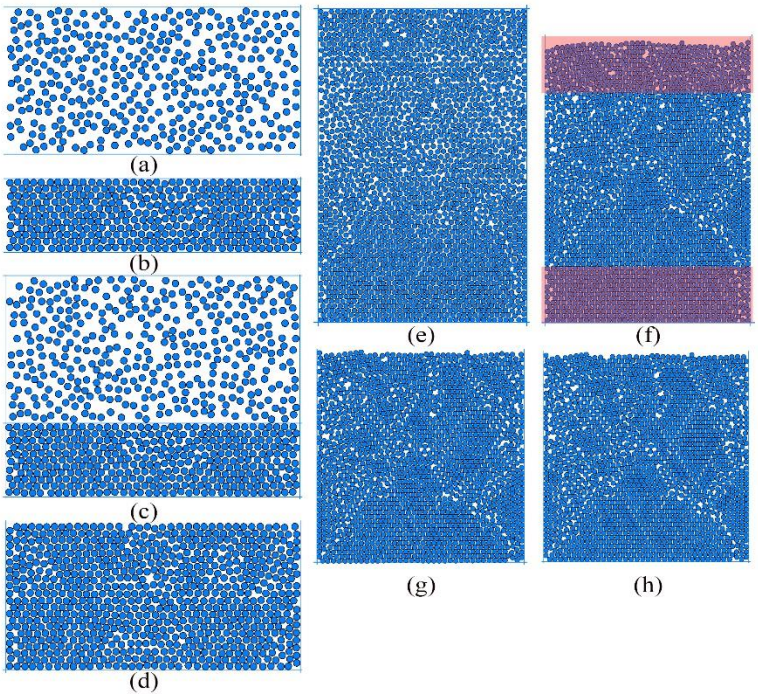


Fig. 2 The procedure of the multi-layer method for generating specimens (a: generating randomly non-overlapping balls in a given area, b: moving down the top wall to a target porosity, c: generating randomly non-overlapping balls in the second given area, d: moving the top wall down to a target porosity to form the second layer of balls, e: six layers of balls, f: calculating to a balanced state under gravity, g: deleting the first and last layers of balls, and h: calculating to a balanced state under gravity)

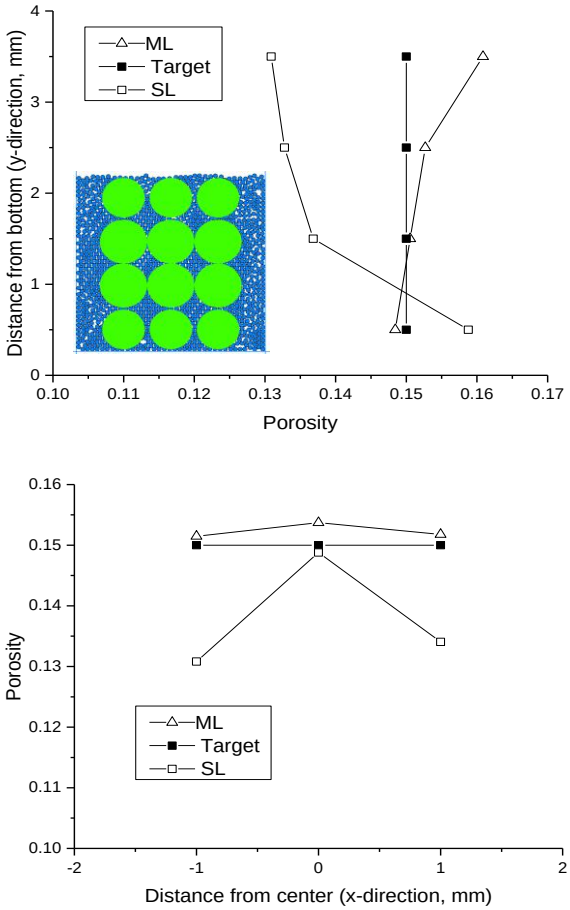


Fig. 3 Distribution of the porosity in specimens obtained by the single layer method and multi-layer method

Table 1 Parameters of the model

| Parameters | Values |
|---|---|
| Normal stiffness of a ball | $10^6$ N/m |
| Tangential stiffness of a ball | $10^6$ N/m |
| Friction of a ball | 0.5-1 |
| Density of a ball | 2650 kg/m$^3$ |
| Normal stiffness of the wall | $10^6$ N/m |
| Tangential stiffness of the wall | $10^6$ N/m |
| Friction of the wall | 0.5 |

convenience of making openings, rectangular walls with ignored heights are used. Then, the balls are driven by gravity to estimate whether a stable soil bridge is formed. The opening on the bottom wall is constantly widened until a stable bridge cannot form. To increase the reliability of the results, every case is calculated three times with three specimens that are generated under the same conditions except for a different random number. The largest opening when a stable bridge can form for the three samples is used to calculate the bridge coefficient (α) according to the following equation:

$$\alpha = \frac{W}{D_{85}} \tag{4}$$

where W is the width of the opening and $D_{85}$ is the characteristic diameter of the soil. When the uniformity coefficient is 1, $D_{85}$ equals the largest diameter of the particles.

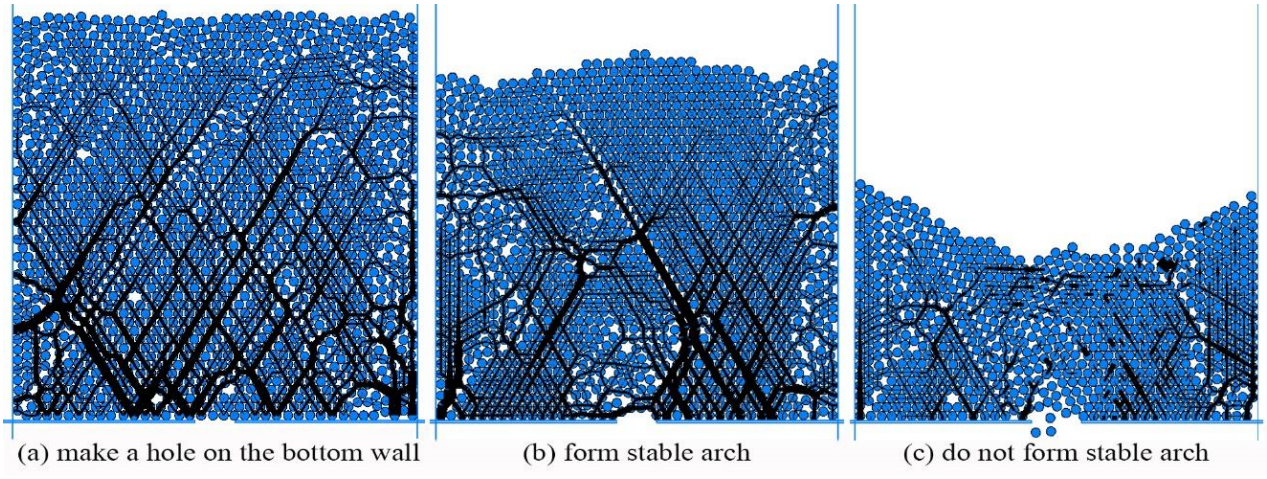


Fig. 4 Simulation process of a soil bridge

For a higher computational efficiency, it is considered that the bridge does not form if the loss rate of the balls (k) is greater than 50%. k is calculated by the following equation:

$$k = \frac{num\_total - num\_now}{num\_total} \tag{5}$$

where num_total represents the total number of balls, and num_now represents the present number of balls.

## 3. Simulation results and discussion

### *3.1 Influence of hydraulic gradient on bridge formation*

In many cases, cohesionless sand is below the groundwater level. If there is a need for filter materials to retain cohesionless sand and drainage, bridge formation will be an important factor that needs to be considered when designing filter materials. To more realistically reflect the bridge formation of cohesionless sand that is below the groundwater level, the influence of water should be considered.

To study the influence of different hydraulic gradients on bridge formation, fluid–solid interactions need to be considered. When fluid flows through particle aggregation, as for a single particle, the forces from the fluid (Huang *et al*. 2014, Zou *et al*. 2013) are composed of a drag force (the first term on the right of Eq. (5)), fluid gradient force (the second term on the right of Eq. (5)) and buoyancy force (the third term on the right of Eq. (5)). For the sake of simplification, the drag force is not considered in this paper (Wang and Ni 2013), and it is relatively small compared with the other forces when the fluid velocity is slow in the seepage field. Only the seepage force and buoyancy force are employed to study the fluid–solid interaction. In addition, an average hydraulic gradient is applied to the whole specimen, and it remains the same during the simulation process; therefore, a weak form of coupling between the fluid and particles is considered.

$$\bar{f}_{fluid} = \frac{4}{3}\pi r^3 \frac{\bar{f}_b}{1-n} + \frac{4}{3}\pi r^3 \nabla p - \frac{4}{3}\pi r^3 \rho_f \bar{g} \tag{5}$$

where $r$ is the radius of the particle, $\vec{f}_b$ is the body force per unit volume, $p$ is the fluid pressure, $\vec{g}$ is the acceleration of gravity and $\rho_f$ is the density of fluid. As the balls used in this paper are two dimensional with a unit thickness, the volume of the ball is calculated by $\pi r^2$.

Four hydraulic gradients (0, 5, 10, 20) were selected in this paper. The specimen is generated with a targeted porosity of 0.15, and the diameters of the particles are the same (0.1 mm). The width and height of the specimen are both set to 4 mm, and they are 40 times that of the diameter of the particles. The influence of the walls can be ignored when the walls are more than 15 times that of the diameter of the particles away from the opening (Mondal and Sharma 2014). The friction coefficient of the particles is set to 0.5, and the remaining parameters of the specimen are given in Table 1. To increase the reliability of the results, every case is simulated three times with three specimens that are generated under the same conditions except for a different random number. The final porosity of every specimen is slightly different from its design value due to randomness. During the calculation, only one opening is made at the bottom wall. The simulated results are presented in Table 2, and the accuracy of the bridge coefficient is within 0.01.

When the hydraulic gradient was zero, the bridge coefficient was 4.47, and it remained the same when the hydraulic gradient increased to 5. As the hydraulic gradient continued to increase, the bridge coefficient dropped to 4.34 ($i$=20). This shows that the hydraulic gradient decreased the bridge coefficient, and the effect was more substantial when the value of the hydraulic gradient was large. This is because the force applied to the particles by water drove the particles to move downward, which was unfavourable to the formation of a soil bridge. It is inferred that the opposite effect would be observed if the water flowed upward. In conclusion, the hydraulic gradient had an important effect on the bridging behaviour, and it should receive sufficient attention in the design of filter materials for cohesionless sand.

Table 2 Bridge coefficient of the specimens under different hydraulic gradients

| Specimen | Porosity | Diameter of a ball (mm) | Hydraulic gradient | Bridge coefficient α |
|---|---|---|---|---|
| S1 | 0.153 | 0.1 | | |
| S2 | 0.150 | 0.1 | 0 | 4.47 |
| S3 | 0.148 | 0.1 | | |
| S1 | 0.153 | 0.1 | | |
| S2 | 0.150 | 0.1 | 5 | 4.47 |
| S3 | 0.148 | 0.1 | | |
| S1 | 0.153 | 0.1 | | |
| S2 | 0.150 | 0.1 | 10 | 4.45 |
| S3 | 0.148 | 0.1 | | |
| S1 | 0.153 | 0.1 | | |
| S2 | 0.150 | 0.1 | 20 | 4.34 |
| S3 | 0.148 | 0.1 | | |

### *3.2 Influence of the confining pressure on bridge formation*

Cohesionless sand is buried at different depths in the ground; therefore, it is subjected to different confining pressures according to its depth. This section presents the simulated results of the influence of the confining pressure on the bridge formation of cohesionless sand.

As a specimen generated by the ML method is not guaranteed to have a smooth surface, it is inconvenient to apply a confining pressure later. Hence, the specimen is first created by the BDM in a single layer with a diameter of balls of 0.1 mm (the target porosity is 0.20), and the external force is then applied and maintained by four walls with servo control (Zhang *et al*. 2017). The width and height of the specimen are both set to 4 mm, and the friction coefficient of the ball is 0.5. The remaining parameters of the specimen are given in Table 1. During these processes, gravity is not applied to the specimen to enhance its homogeneity until the simulation of the formation of a soil bridge. This is reasonable because the value of gravity is much less than the value of the confining pressure. Three confining pressures (10 kPa, 20 kPa, and 40 kPa) are considered. It should be noted that the final porosity of the specimen is different from the initial value (0.2), as the confining pressure makes the specimen denser. Three specimens are generated for every confining pressure, and their final average porosities are 0.17, 0.15 and 0.11 when the confining pressures are 10 kPa, 20 kPa and 40 kPa, respectively.

During the calculation, only one opening was made at the bottom wall, and all the simulations were executed with a hydraulic gradient of 10. The common largest hydraulic gradient in the lab was 10 (Giroud 2010). The simulated results are presented in Fig. 5, and the accuracy of the bridge coefficient was within 0.1. When the confining pressure was greater than zero, the bridge coefficient was larger than that when the confining pressure was zero. This indicates that a proper confining pressure was favourable to

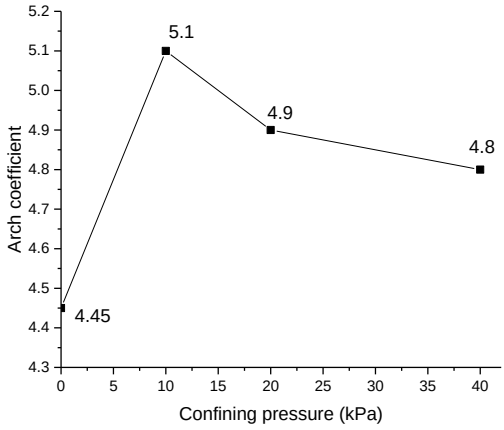


Fig. 5 Bridge coefficient of the specimens under different confining pressures

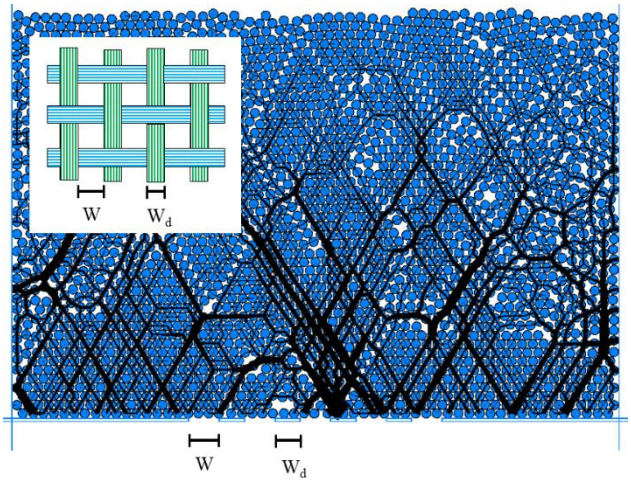


Fig. 6 Schematic diagram of multiple openings

increase the bridge coefficient. As the confining pressure increased from 10 kPa to 40 kPa, the bridge coefficient decreased from 5.1 to 4.8, and the decrease slowed. This shows that with the continual increase in the confining pressure, the confining pressure began to have an unfavourable effect on the formation of a soil bridge. The confining pressure had two effects on the soil bridge. On the one hand, the compactness effect of the confining pressure increased the internal locking of the soil particles. As a result, it was easier to form a soil bridge. On the other hand, with the continual increase in the confining pressure, it would lead to the sliding of the soil particles, which was unfavourable to the formation of a soil bridge.

### *3.3 Influence of multiple openings on the bridge formation*

In projects, there are more than one opening during the formation of a soil bridge. Therefore, the influence of multiple openings on the bridge formation of cohesionless sand is studied in this section. The ratio of the width of the opening (W) and the distance between two openings ($W_d$) is an important parameter that needs to be determined. Because geotextiles are widely used as filter materials for cohesionless sand, the ratio is determined based on the

Table 3 Bridge coefficient of the specimens under different numbers of openings

| Specimen | Porosity | Diameter of a ball (mm) | Hydraulic gradient | Number of openings | $W/W_d$ | bridge coefficient α |
|---|---|---|---|---|---|---|
| S1 | 0.153 | 0.1 | | | | |
| S2 | 0.150 | 0.1 | 10 | single | / | 4.45 |
| S3 | 0.148 | 0.1 | | | | |
| S4 | 0.148 | 0.1 | | | | |
| S5 | 0.150 | 0.1 | 10 | Multiple | 1.5 | 2.84 |
| S6 | 0.152 | 0.1 | | | | |
| S4 | 0.148 | 0.1 | | | | |
| S5 | 0.150 | 0.1 | 10 | Multiple | 1.2 | 2.86 |
| S6 | 0.152 | 0.1 | | | | |

characteristics of geotextiles. Two ratios (1.5 and 1.2) are selected according to (Yan *et al*. 2020), and five openings are made at the bottom wall (Fig. 6).

The specimen was generated with a targeted porosity of 0.15, and the diameters of the particles were the same (0.1 mm). To ensure that the lateral walls were more than 15 times that of the diameter of the particles away from the openings, the width and height of the specimen were set to 6 mm and 4 mm, respectively. The friction coefficient of the particles was set to 0.5, and the remaining parameters of the specimen are given in Table 1. Three specimens were generated under the same conditions except for a different random number, and all the simulations were executed with a hydraulic gradient of 10.

The simulated results are given in Table 3. It is clear that the bridge coefficient substantially decreased when there was more than one opening. This shows that the number of openings had a substantial influence on the formation of the soil bridge. In addition, as the ratio of the width of the opening and the distance between two openings increased from 1.2 to 1.5, the bridge coefficient dropped from 2.86 to 2.84. The wall at the bottom played an important role in the formation of the soil bridge, which could offer support for the bridge foot. The narrower walls decreased this effect of the support; as a result, it was more difficult for the bridge to form. It is recommended that the actual opening condition should be adopted to study bridge formation in future research.

### *3.4 Influence of the inherent characteristics of cohesionless sand on bridge formation*

Inherent characteristics of cohesionless sand, such as the porosity, gradation and friction coefficient, also have an important influence on bridge formation. This section describes the simulated results of cohesionless sand with different porosities, gradations and friction coefficients.

#### *3.4.1 Porosity*

According to Wang *et al*. (2014), the common porosity of the 2-D model varied from 0.15 to 0.20. Hence, three porosities (0.150, 0.175 and 0.194) were selected to study the influence of compactness on the bridge formation of cohesionless sand. The specimen was generated with a friction coefficient of 0.5, and the diameters of the particles were the same (0.1 mm). The width and height of the specimen were both set to 4 mm, and the remaining parameters of the specimen are given in Table 1. Three specimens were generated under the same conditions except for a different random number, and all the simulations were executed with a hydraulic gradient of 10. During the calculation, only one opening was made at the bottom wall, and the simulated results are given in Table 4. It is clear that with increasing porosity, the bridge coefficient experienced a slight decline. When the porosity changed from 0.175 to 0.194, the bridge coefficient only declined by 0.01. When the porosity gradually increased, the cohesionless sand became looser. This decreased the internal locking of the soil particles. As a result, it was more difficult to form soil bridges. As a whole, the influence of the porosity on the bridge coefficient was small.

Table 4 Bridge coefficient of the specimens under different porosities

| Specimen | Porosity | Diameter of a ball (mm) | Average porosity | Hydraulic gradient | Bridge coefficient α |
|---|---|---|---|---|---|
| S1 | 0.153 | 0.1 | | | |
| S2 | 0.150 | 0.1 | 0.150 | 10 | 4.45 |
| S3 | 0.148 | 0.1 | | | |
| S7 | 0.172 | 0.1 | | | |
| S8 | 0.175 | 0.1 | 0.175 | 10 | 4.28 |
| S9 | 0.178 | 0.1 | | | |
| S10 | 0.193 | 0.1 | | | |
| S11 | 0.194 | 0.1 | 0.194 | 10 | 4.27 |
| S12 | 0.195 | 0.1 | | | |

Table 5 Particle gradation of the cohesionless sand

| Cu ($d_{60}/d_{10}$) | $D_{min}$ /mm | $D_{10}$ /mm | $D_{15}$ /mm | $D_{60}$ /mm | $D_{max}$ /mm |
|---|---|---|---|---|---|
| 1.65 | 0.10 | 0.115 | 0.12 | 0.19 | 0.25 |
| 2.50 | 0.095 | 0.10 | 0.12 | 0.25 | 0.30 |

#### *3.4.2 Gradation*

The uniformity coefficient ($Cu= d_{60}/d_{10}$) is an important parameter for describing different gradations of cohesionless sand. Two Cu values of 1.65 and 2.5 are considered in this paper, and the specific gradation is given in Table 5. When the particles have the same diameter, Cu is 1, and this case is chosen as the control case.

The specimen was generated with a targeted porosity of 0.15, and the diameters of the particles were the same (0.1 mm). The width and height of the specimen were both set to 4 mm, and the friction coefficient of the particles was set to 0.5. The remaining parameters of the specimen are given in Table 1. Three specimens were generated under the same conditions except for a different random number, and all the simulations were executed with a hydraulic gradient of 10. Only one opening was made at the bottom wall, and the simulated results are given in Table 6.

When Cu increased from 1.0 to 1.65, the bridge coefficient experienced a remarkable decline from 4.45 to 3.25. The bridge coefficient was 3.0 when Cu was 2.5. Therefore, the gradation of the cohesionless sand had a

Table 6 Bridge coefficient of the specimens under different gradations

| Specimen | Porosity | Diameter of a ball (mm) | Cu | Hydraulic gradient | Bridge coefficient α |
|---|---|---|---|---|---|
| S1 | 0.153 | 0.1 | | | |
| S2 | 0.150 | 0.1 | 1.00 | 10 | 4.45 |
| S3 | 0.148 | 0.1 | | | |
| S12 | 0.150 | 0.1 | | | |
| S14 | 0.152 | 0.1 | 1.65 | 10 | 3.25 |
| S15 | 0.152 | 0.1 | | | |
| S16 | 0.148 | 0.1 | | | |
| S17 | 0.150 | 0.1 | 2.50 | 10 | 3.00 |
| S18 | 0.150 | 0.1 | | | |

substantial influence on the formation of the soil bridge. With the increase in the uniformity coefficient, the structure of the cohesionless sand became more unstable. In addition, it was more different for the soil bridge to form.

### *3.4.3 Friction coefficient and diameter*

All the simulations described above used a friction coefficient of sand of 0.5. The friction coefficient of sand in S1 to S3 was changed to 1.0, and these specimens were used to execute a simulation with one opening and a hydraulic gradient of 10. The bridge coefficient was 4.47, which was slightly larger than that (4.45) when the friction coefficient was 0.5; therefore, a larger friction coefficient of cohesionless sand was conducive to the formation of a soil bridge.

Except for specimens S12 to S18, the diameter of the cohesionless sand was set as 0.5 mm for the remaining specimens (Cu=1). To determine whether the conclusions obtained by these specimens were applicable to other diameters of cohesionless sand (Cu=1), three specimens were generated with a particle diameter of 1 mm. The targeted porosity of the specimen was 0.15, and the friction coefficient of the particles was 0.5. The width and height of the specimen were both set to 4 mm, and the remaining parameters of the specimen are given in Table 1. Only one opening was made at the bottom wall, and the average hydraulic gradient was 10. The bridge coefficient (4.45) was identical to that of the specimen with a particle diameter of 0.5 mm. This shows that when Cu=1, the conclusions obtained by one particle diameter were applicable to specimens with different particle diameters.

## 4. Conclusions

To understand bridge formation at the cohesionless sand-geotextile interface under different conditions, a series of numerical simulations with the two-dimensional DEM were conducted and found: The number of openings of the filter had a substantial influence on the formation of the soil bridge, and the bridge coefficient substantially decreased when there was more than one opening. Because the narrower walls decreased the support of the bridge foot, it was more difficult for the bridge to form. It is recommended that the actual opening condition should be adopted to study the formation of bridges in future research.

When the uniformity coefficient increased from 1.0 to 1.65, the bridge coefficient experienced a remarkable decline from 4.45 to 3.25. The gradation of the cohesionless sand had a substantial influence on the formation of the soil bridge. With the increase in the uniformity coefficient, the structure of the cohesionless sand became more unstable, and it was more different for the formation of the soil bridge.

When the confining pressure was greater than zero, the bridge coefficient was larger than that when there was no confining pressure. With the continual increase in the confining pressure, the confining pressure began to have an unfavourable effect on the formation of a soil bridge.

The hydraulic gradient slightly decreased the bridge coefficient when the uniformity coefficient was 1, and the effect was more substantial when the value of the hydraulic gradient was large. As a whole, the influence of the porosity and the friction coefficient of sand on the bridge coefficient was small when the degradation of the cohesionless sand was uniform. A smaller porosity and larger friction coefficient were conducive to the formation of soil bridges.

## Acknowledgements

This paper was supported by “the National Natural Science Foundation of China” (Grant No. 51609069) and “the National Key Research and Development Program of China” (Grant No. 2017YFC1502603).

## Notations

| | |
|---|---|
| Cu | coefficient of uniformity (dimensionless) |
| $d_X$ | soil particle size corresponding to $X$% passing (mm) |
| $D_0$ | the average pore diameter of the filter material (mm) |
| $d_k$ | the controlling diameter of the protected soil (mm) |
| α | bridge coefficient (dimensionless) |
| W | width of the opening (mm) |
| $W_d$ | the distance between two openings (mm) |
| k | the loss rate of balls (dimensionless) |
| num_total | the total number of balls |
| num_now | the number of balls at present in the model |
| $i$ | hydraulic gradient (dimensionless) |

## References

Cundall, P.A. (1971), “A computer model for simulating progressive, large-scale movements in blocky rock systems”, *The Symposium of the International Society of Rock Mechanics*, Nancy, October.

Cundall, P.A. (1988), “Formulation of a three-dimensional distinct element model—Part I. a scheme to detect and represent contacts in a system composed of many polyhedral blocks”, *J. Rock Mech. Mining Sci. Geomech. Abstracts*, **25**(3), 107-116. https://doi.org/10.1016/0148-9062(88)92293-0.

Cundall, P.A. and Strack, O.D.L. (1979), “A discrete numerical model for granular assemblies”, *Geotechnique*, **29**(1), 47-65.

https://doi.org/10.1680/geot.1979.29.1.47.

Giroud, J.P. (2010), "Development of criteria for geotextile and granular filters", *Proceedings of the 9th International Conference on Geosynthetics*, Guarujá, May.

Guerrero, B.V., Chakraborty, B., Zuriguel, I. and Garcimartin, A. (2019), "Nonergodicity in silo unclogging: Broken and unbroken arches", *Phys. Review E*, **100**(3), 032901. https://doi.org/10.1103/PhysRevE.100.032901.

Hart, R., Cundall, P.A. and Lemos, J. (1988), "Formulation of a three-dimensional distinct element model—Part II. mechanical calculations for motion and interaction of a system composed of many polyhedral blocks", *J. Rock Mech. Mining Sci. Geomech. Abstracts*, **25**(3), 117-125. https://doi.org/10.1016/0148-9062(88)92294-2.

Huang, Q., Zhan, M., Sheng, J., Luo, Y. and Su, B. (2014), "Investigation of fluid flow-induced particle migration in granular filters using a DEM-CFD method", *J. Hydrodynam.*, **26**(3), 406-415. https://doi.org/10.1016/s1001-6058(14)60046-9.

Jung, J., Cao, S.C., Shin, Y.H., Al-Raoush, R.I., Alshibli, K. and Choi, J.W. (2018), "A microfluidic pore model to study the migration of fine particles in single-phase and multi-phase flows in porous media", *Microsyst. Technol.-Micro-and-Nanosyst.-Info. Storage Process. Syst.*, **24**(2), 1071-1080. https://doi.org/10.1007/s00542-017-3462-1.

Khan, M.W., Dawson, A.R. and Marshall, A.M. (2018), "A dynamic gradient ratio test apparatus", *Geotext. Geomembr.*, **46**(6), 782-789. https://doi.org/10.1016/j.geotexmem.2018.07.003.

Li, L. and Aubertin, M. (2009a), "Horizontal pressure on barricades for backfilled stopes. Part I: Fully drained conditions", *Canadian Geotech. J.*, **46**(1), 37-46. https://doi.org/10.1139/t08-104.

Li, L. and Aubertin, M. (2009b), "A three-dimensional analysis of the total and effective stresses in submerged backfilled stopes", *Geotech. Geological Eng.*, **27**(4), 559-569. https://doi.org/10.1007/s10706-009-9257-0.

Li, X., Qi, Y., Tang, X. and Gao, Q. (2017), "Simulation of base soil-filter system with two typical gradations based on PFC", *J. Yangtze River Sci. Res. Institute*, **34**(4), 92-97. (In Chinese).

Liu, J. and Xie, D. (2017), "Design principles and guidelines of filters", *Chinese J. Geotech. Eng.*, **39**(4), 609-616. (In Chinese)

Liu, Q., Zhao, B. and Santamarina, J.C. (2019), "Particle migration and clogging in porous media: a convergent flow microfluidics study", *J. Geophys. Res. Solid Earth*, **124**(9), 9495-9504. https://doi.org/10.1029/2019jb017813.

Liu, S., Wang, Y., and Feng, D. (2021), "Compatibility of tailings–nonwoven geotextile under stress and the effect of sand filter", *Geosynth. Int.*, **28**(2), 206-213. https://doi.10.1680/jgein.20.00046.

Lozano, C., Zuriguel, I. and Garcimartin, A. (2015), "Stability of clogging arches in a silo submitted to vertical vibrations", *Phys. Review E*, **91**(6), 062203. https://doi.org/10.1103/PhysRevE.91.062203.

Mondal, S. and Sharma, M.M. (2014), "Role of flying buttresses in the jamming of granular matter through multiple rectangular outlets", *Granular Matter*, **16**(1), 125-132. https://doi.org/10.1007/s10035-013-0461-5.

Parretta, A. and Grillo, P. (2019), "Flow dynamics of spherical grains through conical cardboard hoppers", *Granular Matter*, **21**(2), 1-22. https://doi.org/10.1007/s10035-019-0884-8.

Raja, M.N.A. and Shukla, S.K. (2020), "Ultimate bearing capacity of strip footing resting on soil bed strengthened by wraparound geosynthetic reinforcement technique", *Geotext. Geomembr.*, **48**(6), 867-874. https://doi.https://doi.org/10.1016/j.geotexmem.2020.06.005.

Raja, M.N.A. and Shukla, S.K. (2021a) "Experimental study on repeatedly loaded foundation soil strengthened by wraparound geosynthetic reinforcement technique", *J. Rock Mech. Geotech. Eng.*, **13**(4), 899-911. https://doi.https://doi.org/10.1016/j.jrmge.2021.02.001.

Raja, M.N.A. and Shukla, S.K. (2021b), "Predicting the settlement of geosynthetic-reinforced soil foundations using evolutionary artificial intelligence technique", *Geotext. Geomembr.*, **49**(5), 1280-1293. https://doi.https://doi.org/10.1016/j.geotexmem.2021.04.007.

Valdes, J.R. and Santamarina, J.C. (2006), "Particle clogging in radial flow: microscale mechanisms", *SPE J.*, **11**(2), 193-198. https://doi.org/10.2118/88819-pa.

Valdes, J.R. and Santamarina, J.C. (2008), "Clogging: bridge formation and vibration-based destabilization", *Canadian Geotech. J.*, **45**(2), 177-184. https://doi.org/10.1139/t07-088.

Wang, Y. and Ni, X. (2013), "Hydro-mechanical analysis of piping erosion based on similarity criterion at micro-level by PFC3D", *European J. Environ. Civil Eng.*, **17**, S187-S204. https://doi.org/10.1080/19648189.2013.834594.

Wang, Z.J., Ruiken, A., Jacobs, F. and Ziegler, M. (2014), "A new suggestion for determining 2D porosities in DEM studies", *Geomech. Eng.*, **7**(6), 665-678. https://doi.org/10.12989/gae.2014.7.6.665.

Watson, P.D.J. and John, N.W.M. (1999), "Geotextile filter design and simulated bridge formation at the soil–geotextile interface", *Geotext. Geomembr.*, **17**(5), 265-280. https://doi.org/10.1016/S0266-1144(99)00013-8.

Xu, C., Liang, L., Chen, Q., Luo, W. and Chen, Y.F. (2019a), "Experimental study of soil arching effect under seepage condition", *Acta Geotechnica*, **14**(6), 2031-2044. https://doi.org/10.1007/s11440-019-00769-y.

Xu, C., Zhang, X., Han, J. and Yang, Y. (2019b), "Two-dimensional soil-arching behavior under static and cyclic loading", *Int. J. Geomech.*, **19**(8), 04019091. https://doi.org/10.1061/(asce)gm.1943-5622.0001482.

Yan, C., Yunchu, Y. and Jiangrui, Q. (2020), "Mathematical modeling on effective thermal conductivity of woven fabrics based on structural parameters", *Adv. Textile Technol.*, 1-10. (In Chinese)

Zhang, H., Guo, H., Shi, T., Ye, M., Huang, H. and Li, Z. (2017), "Cyclic loading tests on ceramic breeder pebble bed by discrete element modeling", *Fusion Eng. Design*, **118**, 40-44. https://doi.org/10.1016/j.fusengdes.2017.02.044.

Zou, Y.-H., Chen, Q., Chen, X.-Q. and Cui, P. (2013), "Discrete numerical modeling of particle transport in granular filters", *Comput. Geotech.*, **47**, 48-56. https://doi.org/10.1016/j.compgeo.2012.06.002.

*GC*